Monitoring and Prediction of Drought Using Remote Sensing Indices, Meteorological Indices, and QGIS Platform with Integration of an XGBoost Model: Case Study of Tigrigra Plain (Azrou Region, Middle Atlas)

Fangour Anass*[1], Idrissi Mounadi Doha*[1], Ziani Ayah*[1], Harib Douaa*[1], Mahi iliasse*[1], Ouamam Achraf*[2], Rhinane Hassan*[1], Agharroud Kamal*[1], Farah Saad*[1]

[1]Department of Geology, Faculty of Sciences Ain Chock, University Hassan II, Casablanca 20100, Morocco.

[2]Agronomic and Veterinary Institute Hassan II, Rabat, Morocco

ABSTRACT

This study aims to leverage spatial remote sensing technologies, particularly by integrating artificial intelligence models with a Geographic Information System (GIS) and various influential parameters, for drought monitoring. We evaluated the spatial extent of drought in the Tigrigra watershed using Landsat 5, Landsat 7, and Landsat 8 datasets for each season over a 20-year period (from 2000 to 2022). Additionally, we sought to characterize the spatiotemporal model of drought conditions using the Standardized Precipitation Index (SPI), Vegetation Condition Index (VCI), Temperature Condition Index (TCI), and Vegetation Health Index (VHI). The results reveal episodes of drought ranging from severe to extreme in 2003, 2006, 2007, 2008, 2012, 2016, 2019, and 2021, with specific stations experiencing intensified drought conditions at different time scales. Particularly, the VCI indicates that only 20% of the total area is free from drought, while the TCI highlights an incidence of drought affecting 50% of the northeast part. Similarly, the VHI indicates an incidence of drought affecting 70% of the northeast zone. However, after processing all the indices, we found that the southeastern and southwestern regions exhibit extreme and severe drought, contrasting with the absence of drought in the northeast and northwest. For the years to come, we found that the southeastern and southwestern regions continue to show severe and extreme drought conditions, while the northeastern and northwestern zones are predicted to remain largely free from drought. These findings underscore the necessity for targeted drought mitigation strategies, especially in the more vulnerable southern regions of the Tigrigra watershed.

KEYWORDS: Geographic Information System; Remote Sensing; Artificial Intelligence; Drought.

INTRODUCTION

One of nature's biggest calamities, droughts have a devastating effect on the environment, natural resources, agriculture, society, and economy. Long periods without precipitation during a drought result in a significant reduction in water availability. The most widely used hydrometeorological drought indices are the Palmer Index (Palmer, 1965), the Standardized Precipitation Index (SPI) (McKee et al., 1993), the Surface Water Supply Index (Shafer, 1982), the Streamflow Drought Index (Nalbantis and Tsakiris, 2009), the Standardized Hydrological Index (Sharma and Panu, 2010), the Standardized Evapotranspiration Index (Vicente-Serrano et al., 2010), and the Agricultural Reference Drought Index (Woli et al., 2012). Numerous other hydrometeorological drought indices are also available to measure droughts.

Many of the indices used to quantify hydrological droughts require large datasets and complex computations, in contrast to the simpler and more effective meteorological drought indices such as the SPI (Nalbantis and Tsakiris, 2009).

Accurately estimating drought in arid and hyper-arid regions is particularly challenging due to the sparse distribution of meteorological stations and the accompanying uncertainties. This issue may be further complicated by natural barriers such as sand dunes and mountains (Hereher et al., 2020). However, by the end of the 20th century, advances in remote sensing and Earth observation technology had significantly improved drought monitoring, thanks in part to the National Aeronautics and Space Administration’s (NASA) 1972 launch of the Landsat series (West et al., 2019).

Furthermore, the rising temperatures caused by climate change have increased awareness and interest in understanding its effects. Consequently, experts in geospatial science now view remote sensing as a vital tool for providing the information needed to assess ecosystem conditions and monitor sudden changes in climate both temporally and spatially (Sarkar et al., 2020). To address the lack of data and the limited use of remote sensing and GIS technologies in drought monitoring, this study aims to create a drought risk map by integrating influential factors using GIS techniques. The objectives include: (1) assessing the spatial extent of drought in the Tigrigra watershed for each four-year season (from 2000 to 2022) using Landsat 5, Landsat 7, and Landsat 8 datasets; (2) characterizing the spatiotemporal pattern of drought conditions using SPI, VCI, TCI, and VHI indices. This research will be valuable for urban planners and environmental scientists, enabling them to make informed decisions and implement policies aimed at mitigating drought in the Tigrigra watershed.

Site description

The watershed of the Tigrigra River is delineated on a topographic background. It is located at the confluence of the Central Middle Atlas with the central plateau. It extends between parallels 33°36 and 33°12 N and longitudes 5°34 and 5°06 W. The Tigrigra watershed has an area of 1109 km2 and a perimeter of 211 km. It is situated at

the confluence of the Central Middle Atlas with the central plateau. The watershed presents varied relief, with altitudes ranging between 785 and 2196 m. Its elongated shape follows a NW-SE orientation, and it is delimited by:

- To the Northwest by the causse of Agouray and Adarouch, which runs eastwards towards the confluence of Tigrigra with the Beht River;

- To the Northeast by the causse of El Hajeb and the causse of Ifrane;

- To the East by Michlifène, Jbel Hebri;

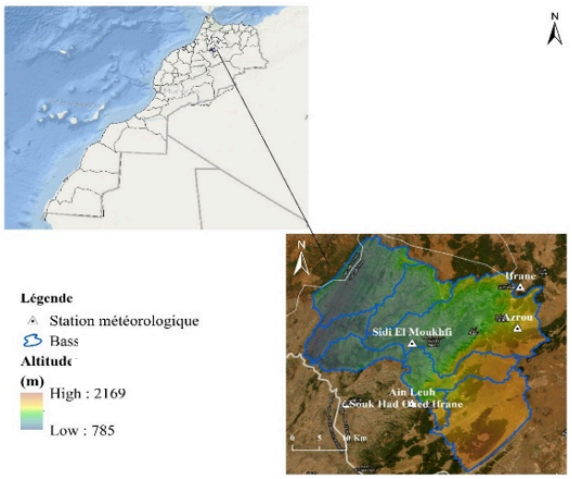

***Fig. 1**: Location of the site.*

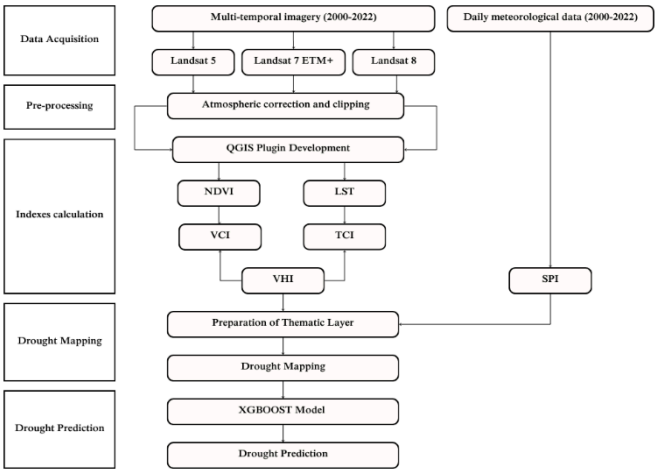

***Fig. 2**: Methodology adopted in this study*

Methods

Five conditioning parameters were used to determine drought in the study areas: Normalized Difference Vegetation Index (NDVI), land surface temperature (LST), Temperature Condition Index (TCI), Vegetation Condition Index (VCI), and Vegetation Health Index (VHI). The Analytical Hierarchy Process (AHP) was employed to perform this process. To make the raw data usable, preprocessing is conducted before generating drought indices. The methodology of this study can be divided into several stages, such as acquiring meteorological data, collecting satellite data, and monitoring meteorological drought using the SPI index. Additionally, monitoring the state of drought is done using drought indices derived from remote sensing such as VCI, TCI, and VHI. [Fig 2]

1.1 Acquisition of meteorological data

This study used monthly precipitation data from the Sebou Basin Hydraulic Agency (ABHS) and global meteorological data from the Soil and Water Assessment Tool. (Global Weather Data for Swat) [2]. The data is from eight meteorological stations. (Agouai; Ain Louh, Ait Aissa, Azrou, El Hajeb, Ifrane, Sidi El Moukhfi, and Souk Had Oued Ifrane) The data from eight meteorological stations located in the Tigrigra plain were collected over a period spanning from 1982 to 2020. (Table 2).

1.2 Acquisition of satellite data

In order to evaluate drought conditions during the previous 20 years (2000–2022) at 4 year intervals, this study uses a multi-step approach (i.e., 2000, 2004,..., and 2022). From 2000 until 2022, satellite photos were gathered for every season. From Path 201 and Row 37, twenty-eight Landsat photos were obtained at Level 1 using the USGS Earth Explorer website. Table 2 presents the specifics of the information gathered from the USGS archive for the following years: 2000, 2004, 2008, 2012, 2016, 2020, and 2022. The USGS provided the Landsat data, which include Thematic Mapper (TM), Enhanced Thematic Mapper Plus (ETM+), and Thermal Infrared Sensor (TIRS) data. The pictures underwent

processing utilizing the Zone 30 North Universal Transverse Mercator (UTM) projection scheme. and the WGS-1984 reference system were applied to the Landsat data.

The indices used in this study include the Normalized Difference Vegetation Index (NDVI), Temperature Condition Index (TCI), Vegetation Condition Index (VCI), Land Surface Temperature (LST), and Vegetation Health Index (VHI). Advanced preprocessing techniques such as radiometric and atmospheric correction were applied to the images to improve their quality and precision before analysis. These Landsat 5, Landsat 7, and Landsat 8 images are corrected to remove atmospheric effects and normalize the data. Subsequently, the indices are calculated to assess vegetation density, changes in plant health, and to monitor drought conditions using satellite imagery.

Satellite image	**sensor**	**spatial resolution**	**Acquisition date**	
Landsat 5	ETM	30 m	31/03/2000	**2000**
			06/08/2000	
			23/09/2000	
			26/11/2000	
			03/04/2004	**2004**
			25/08/2004	
			13/11/2004	
			31/12/2004	
Landsat 7	ETM+	30 m	17/01/2008	**2008**
			29/03/2008	
			20/08/2008	
			24/11/2008	
			16/03/2012	**2012**
			23/08/2012	
			08/09/2012	
			29/12/2012	
			14/05/2016	**2016**
			17/07/2016	
			21/10/2016	
			24/12/2016	
			07/04/2020	**2020**
			13/08/2020	
			16/10/2020	
			17/11/2020	
Landsat 8	OLI+	30 m	29/04/2022	**2022**
			19/08/2022	
			14/10/2022	
			25/12/2022	

Table 1: *Satellite images used to calculate the various indices.*

1.3 Standardized Precipitation Index (SPI)

The SPI index for the research region was calculated using a monthly rainfall database that was created. This database spans 35 years, from 2000 to 2022 (Table 2). The majority of the data came from the Sebou Basin Hydraulic Agency (ABHS), with further data coming from worldwide meteorological sources made available by the Soil and Water Assessment Tool (SWAT) [2]. Eight weather stations, Agouai, Ain Louh, Ait Aissa, Azrou, El Hajeb, Ifrane, Sidi El Moukhfi, and Souk Had Oued Ifrane, were taken into consideration for this investigation (Fig 3).

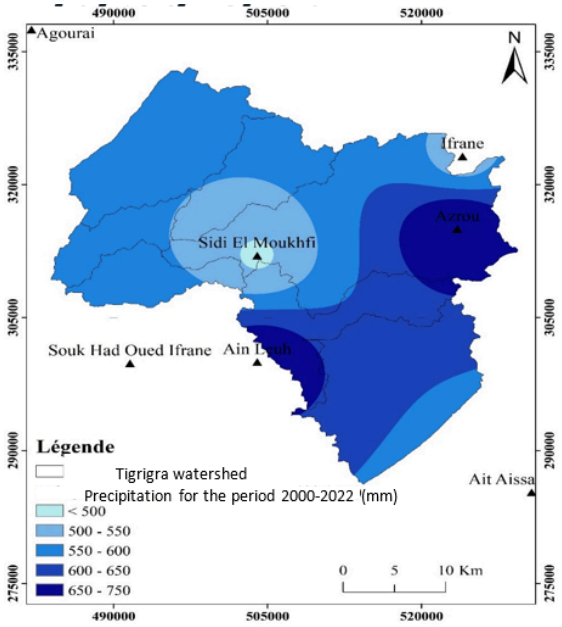

***Fig. 3**: Average yearly rainfall (2000-2022) at studied stations.*

Created by McKee et al. (1993), the Standardized Precipitation Indicator (SPI) is a very basic indicator. The World Meteorological Organization (WMO) suggested this reference index in 2009 to help with climate risk management and drought monitoring. Regardless of the time period taken into consideration, the SPI is a normalized monthly indicator based on the probability of precipitation (P) happening. The formula for it is as follows:

$$SPI = \frac{P_i - P_m}{\sigma}$$

Pi stands for the rainfall in the current month or year, Pm for the series' average rainfall during the time period under consideration, and σ for the series' standard deviation over the same time period.

For every station, the SPI can be computed at several time intervals (1, 3, 6, and 12 months). Utilizing monthly precipitation data, SPI-1 is computed. SPI-3 is computed as the moving average of precipitation over a three-month period, averaged over three months. Other indices for six and twelve months can be computed in a similar manner. While the SPI-3 and SPI-6 indices are typically used to track seasonal fluctuations in drought, the SPI-1 index is helpful for examining short-term differences in the frequency and severity of droughts. On the other hand, the SPI-12 index is helpful in examining the yearly pattern of drought. The index, which contrasts actual precipitation with the volume of water lost through transpiration and evaporation during a specific time period, can be used to determine the severity of a drought.

For every station, the SPI can be computed at several time intervals (1, 3, 6, and 12 months). Utilizing monthly precipitation data, SPI-1 is computed. SPI-3 is computed as the moving average of precipitation over a three-month period, averaged over three months. Other indices for six and twelve months can be computed in a similar manner. When examining short-term fluctuations in the frequency and intensity of droughts, the SPI-1 indicator is helpful. Seasonal fluctuations in drought are often tracked using the SPI-3 and SPI-6 indexes.

On the other hand, the SPI-12 index is helpful in examining the yearly pattern of drought. The index, which contrasts actual precipitation with the volume of water lost through transpiration and evaporation during a specific time period, can be used to determine the severity of a drought.

When the SPI is consistently negative and hits an intensity of -1 or below, it is considered to be in a drought, which ends when the SPI turns positive. Based on the results of this indicator, a drought categorization is carried out (Table 2).

***Table 2**: Classification of drought based on the Standardized Precipitation Index (SPI) value (Mckee et al. (1993))*

SPI class	Drought severity level
$SPI \geq 2$	Extremely Wet
$1,5 \leq SPI \leq 1,99$	Very Wet
$1 \leq SPI \leq 1,49$	Moderately Wet
$-\ 0,99 \leq SPI \leq 0,99$	Near Normal
$-\ 1,49 \leq SPI \leq\ -\ 1$	Moderately Dry
$-\ 1,99 \leq SPI \leq\ -\ 1,5$	Very Dry
$SPI \leq\ -\ 2$	Extremely Dry

Remote Sensing Derived Indices

Vegetation Condition Index (VCI)

In order to evaluate the health and vigor of the vegetation in a specific area, remote sensing techniques employ the Vegetation Condition Index (VCI). It is mostly used to track and assess the state of the plants, especially in dry spells or other times when there is a shortage of water (Kogan, 2001). An equation is used to calculate this index.

$$VCI\ (i) = \frac{NDVI_{(i)} - NDVI_{min}}{NDVI_{max} - NDVI_{min}} \times 100$$

As shown in Table 5, the values of VCI range from 0 to 100, with values below 40 indicating drought conditions in the area [45, 55-57]. Red and near-infrared (NIR) bands are used to determine the NDVI, which is provided by Tucker (1979).

$$NDVI = \frac{NIR - RED}{NIR + RED}$$

Temperature Condition Index (TCI)

The Temperature Condition Index (TCI) is a drought index derived from satellite imagery that is used to assess plant stress caused by temperatures and excessive humidity. TCI is an important index for monitoring drought as it provides information on weather conditions that can affect plant health and agricultural production (Singh et al., 2003). It is related to the vegetation's responsiveness to any adverse temperature change. The following formula illustrates the calculation of TCI (Kogan, 1995):

$$TCI\ (i) = \frac{LST_{max} - LST}{LST_{max} - LST_{min}} \times 100$$

The minimum and highest LST (Land Surface Temperature) values in the area are indicated by the values LSTmin and LSTmax. Table 5 shows that TCI values range from 0 to 100, suggesting either ideal thermal conditions for plants or stress.

The Land Surface Temperature (LST) can be computed using the procedures below (Wukelic et al., 1989).

$$L\lambda\ = M_L \times Q_{CAL} + A_l$$

Where Lλ is the spectral radiance at the top of the atmosphere (TOA) in Wm<0xC2><0xB2>sr<0xC2><0xB2>mm<0xC2><0xB2>1, and QCAL is the quantized and calibrated standard product of pixel values (DN). ML is the band−specific multiplicative rescaling factor from metadata (RADIANCE_MULT_BAND_x, where x is the band number). AL is the band−specific additive rescaling factor from metadata (RADIANCE_ADD_BAND_x, where x

is the band number). It is possible to extract each of these variables from the satellite picture metadata file.

The following formula can be used to convert TOA temperature to radiance (Brightness Temperature) (Cao et al., 2008; Carlson et al., 1997):

$$BT = \left(\frac{K_2}{\left(ln\left(\frac{K_1}{L} \right) + 1 \right)} \right) - 273,15$$

Where K1 is the band-specific thermal conversion constant from metadata (K1_CONSTANT_BAND_x, where x is the thermal band number); K2 is the band-specific thermal conversion constant from metadata (K2_CONSTANT_BAND_x, where x is the thermal band number).

The vegetation proportion (Pv) is calculated using the following equation (Sobrino et al., 2004).

$$P_v = \sqrt{\frac{NDVI - NDVI_{min}}{NDVI_{max} - NDVI_{min}}}$$

The emissivity is calculated using the following equation (Weng et al., 2004).

$$\varepsilon = 0,004 \times P_v + 0,986$$

Finally, the LST (Land Surface Temperature) was calculated using the following equation (Kogan et al., 1997).

$$LST = \frac{BT}{\left(1 + \left[\left(\frac{\lambda \times BT}{\rho} \right) \times ln\varepsilon \right] \right)}$$

where ε is the emissivity and λ is the effective wavelength (10.9 µm for band 10 in Landsat 8 data);

A vacuum's speed of light, c, is 2.998 × 10^8 m/s. ρ is equal to h x c/s = 1.4388 x 10−2 m K; s is the Boltzmann constant (1.38 x 10^−23 J/K); h is the Planck constant (6.626 x 10^−34 Js).

The Vegetative Health Index (VHI)

The Vegetative Health Index (VHI), a useful measure of vegetative stress brought on by droughts, is computed using the following equation. It is the weighted sum of the Vegetation Condition Index (VCI) and the Temperature Condition Index (TCI). According to Kogan et al. (2001), there are five groups into which droughts based on VHI are divided. The various drought conditions based on VCI, TCI, and VHI values are displayed in Table 3.

$$VIH = \frac{VCI + TCI}{2}$$

Class VHI/VCI/TCI	Degree of Drought
0 à 10	Extreme Drought
10 à 20	Severe Drought
20 à 30	Moderate Drought
30 à 40	Mild Drought
Plus de 40	No Drought

***Table 3**: Different drought categories for the indices used*

Results and discussion

Evaluation of drought indices

In order to assess the severity and condition of drought in the Tigrigra watershed from 2000 to 2022, various time scales are used: 1, 3, 6, and 12 months for the meteorological drought index (SPI) and remote sensing-derived indices (e.g., VCI, TCI, and VHI).

Standardized Precipitation Index (SPI)

The time series of SPI at various time scales (i.e., 1, 3, 6, and 12 months) at the eight studied stations from 2000 to 2022 in the Tigrigra watershed are shown in Figs. 4 and 5. The analysis of the chronological series reveals severe to extreme drought episodes in 2000, 2003, 2007, 2009, 2014, and SPI-12, while SPI-3 and SPI-1 indicate drought-free conditions.

2019, and 2021 (Fig 4).

free conditions. However, significant fluctuations are observed in the time series of SPI-1 and SPI-3 compared to SPI-6 and SPI-12. Furthermore, the analysis of the chronological series shows severe to extreme drought episodes in 2000, 2003, 2007, 2009, 2014, 2019, and 2021 (Fig 4).

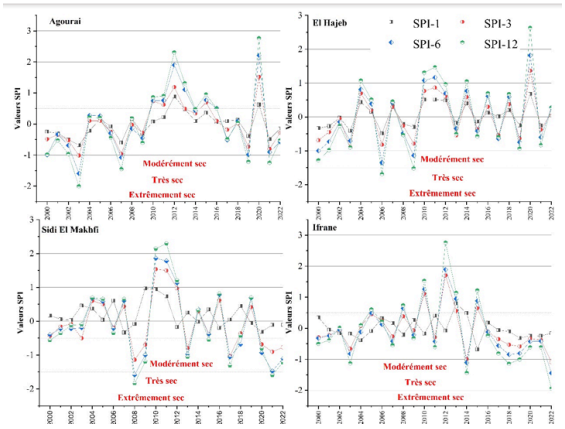

***Fig. 4**: Analysis of the time series of stations in the Tigrigra watershed at different temporal scales of SPI (1, 3, 6, and 12 months)*

Overall, the time series curve presented in Figure 10 shows more severe to extreme drought episodes in 2003, 2006, 2007, 2008, 2012, 2016, 2019, and 2021. Additionally, drought at the Ain Louh station is more severe at the 1, 12, and 6-month scales, followed by SPI-3. Extreme and severe drought episodes at the Ait Aissa station were observed in 2000, 2006, 2008, and 2019. Similarly, severe to extreme drought episodes have been observed at the Azrou station in 2008, 2019, and 2021. Overall, the results (Fig. 5) demonstrate a significant number of extreme and severe drought episodes in 2003, 2007, 2008, 2019, and 2021 in the Tigrigra watershed.

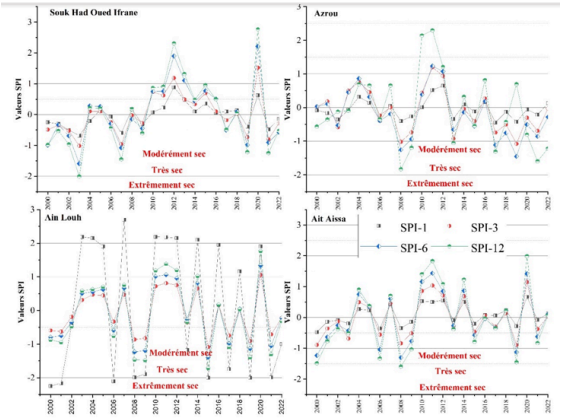

***Fig. 5**: Analysis of the time series of stations in the Tigrigra watershed at different temporal scales of SPI (1, 3, 6, and 12 months)*

*V*egetation Condition Index (VCI)

The yearly average of maps 1 through 28 is represented by maps A through J, which together show the spatial and temporal distribution of the Normalized Difference Vegetation Index (NDVI) in the Tigrigra watershed from 2000 to 2022 in Fig 6. The NDVI shown in Annex A serves as the foundation for these computations. These maps show that during the research period, drought conditions were present in 2004, 2008, 2012, and 2020. Conversely, wetter weather—and hence, comparatively less drought—is noted for the years 2000, 2016, and 2022. It is also noteworthy that the southern portion of the watershed experienced a comparatively greater intensity of drought than the northwest part.

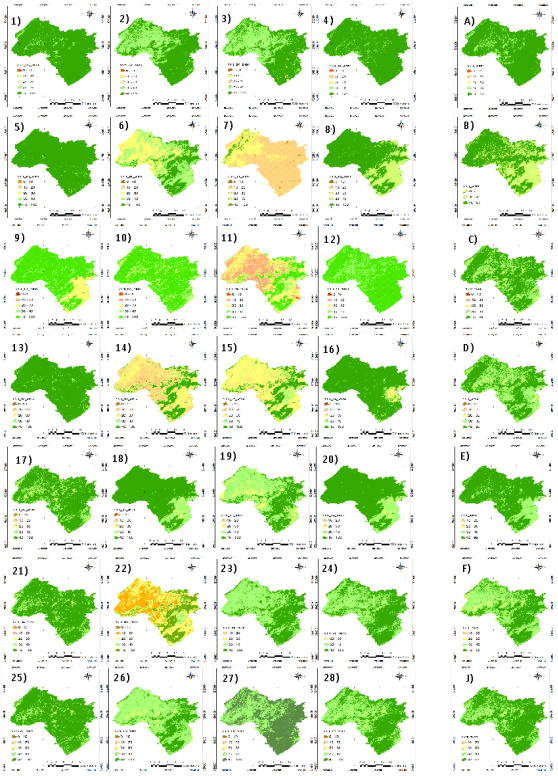

***Fig. 6**: Temporal and spatial distribution of the Vegetation Condition Index.*

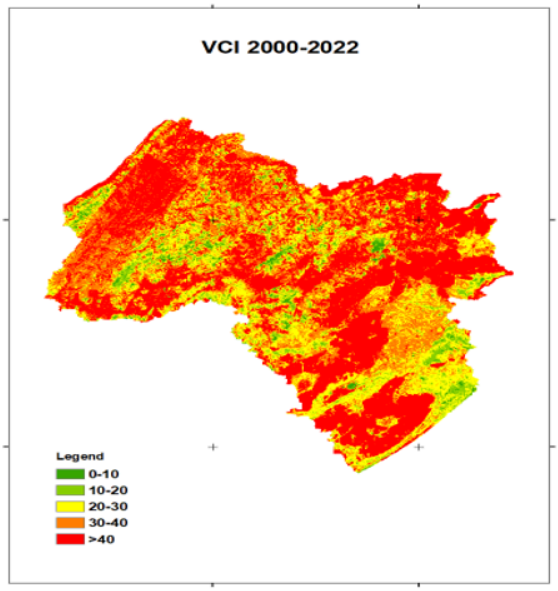

***Fig. 7**: Average VCI from 2000 to 2022*

According to Fig 7, which represents the average of all VCI maps from 2000 to 2022, we find that only 20% of the total area shows a lack of drought.

1.1 Temperature Condition Index (TCI)

Maps A to J provide the annual average of maps 1 to 28, illustrating in Fig 8 the spatial distribution of the Temperature Condition Index (TCI) in the Tigrigra watershed over a 4-year interval from 2000 to 2022, calculated from satellite images. The minimum TCI values are observed in 2000, 2008, 2012, 2016, and 2020, precisely in the northwest part of the study area. TCI has become more severe from 2008 to 2016, especially in the northwest part, where the maximum temperature exceeds 40°C and where annual precipitation is generally reduced. With the exception of a few years (2000, 2012, and 2016), TCI has a geographical distribution trend that is less similar to that of VCI, indicating that TCI is more severe in the northwest than in the south.

The disparity between the VCI and TCI's spatial distributions over specific time periods such as 2000, 2012, and 2016 is mostly attributable to the indices' differing opinions on drought. VCI is computed. from NDVI and only considers the vegetation factor, while TCI is calculated from LST and is an

integrated outcome of numerous variables, such as soil, vegetation, height, precipitation,

topography, and meteorological

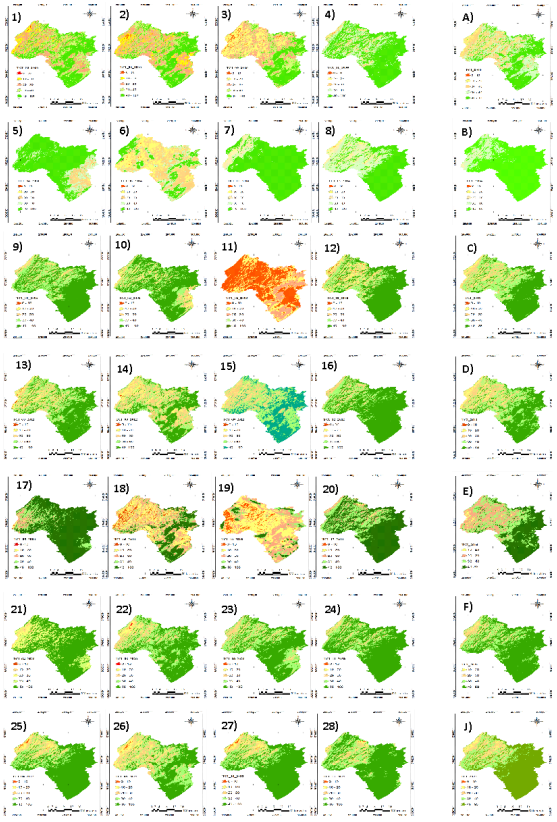

***Fig. 8**: Temporal and spatial distribution of the Temperature Condition Index*

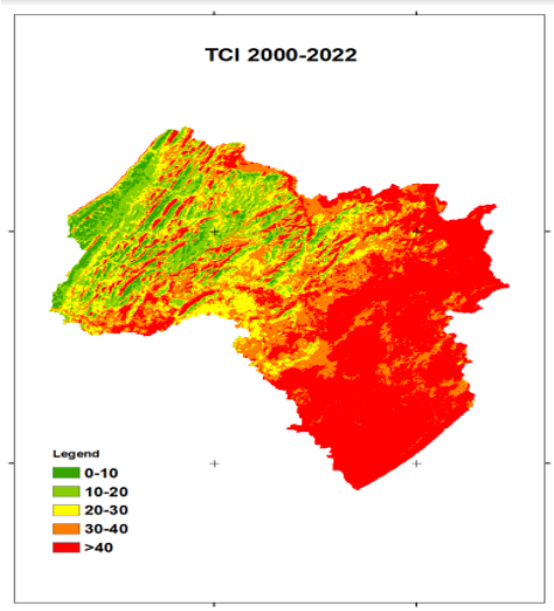

***Fig. 9**: Average TCI from 2000 to 2022*

According to Fig 9, which represents the average of all TCI maps from 2000 to 2022, we find that the northeastern part is affected by drought, with 50% of the area impacted.

1.8 Vegetation Health Index (VHI)

Maps A to J provide the annual average of maps 1 to 28, illustrating in Fig 10. The spatial distribution of the Vegetation Health Index (VHI) in the Tigrigra watershed, obtained respectively from Landsat satellite images, is presented in Figures 25 through 31. Analysis of the results shows that 2000, 2008, 2012, 2016, 2020, and 2022 are the years with the worst drought in the watershed under study. It is important to note, too, that assessments of the drought based on the VHI indicate that it has been worse recently. Additionally, the findings indicate that the northwest is experiencing a severe drought.

Compared to VCI and TCI, the VHI drought index is more extensive. The watershed's northwest regions are particularly susceptible to drought, according to the VHI. In order to address the detrimental effects of drought on the available water resources and agriculture in the northwest region of the Tigrigra watershed, it is important to develop

comprehensive mitigation plans.

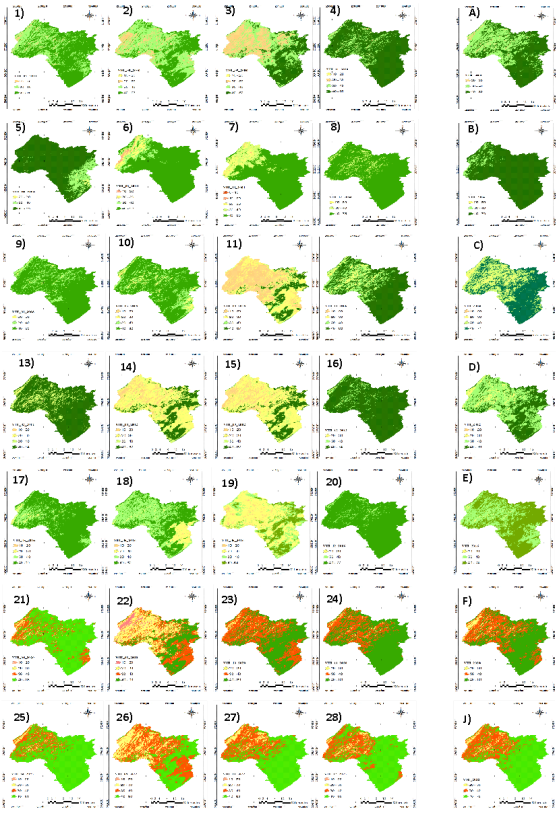

***Fig. 10**: Temporal and spatial distribution of the Vegetation Health Index*

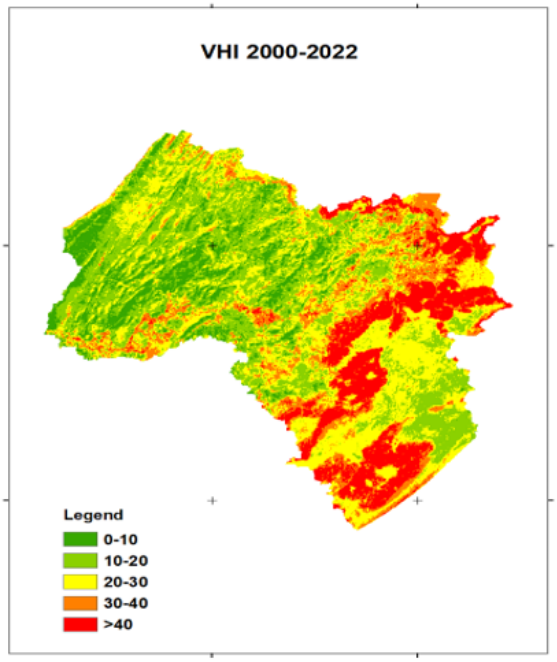

***Fig. 11**: Average VHI from 2000 to 2022*

According to Figure 11, which represents the average of all VHI maps from 2000 to 2022, we observe that the northeast part is affected by drought, with 70% of the area impacted. However, after processing all the indices, we need to determine a reliable value that adapts to all the selected indices.

In conclusion, the results suggest a temporal variation of drought with periods of varying severity. However, a general trend towards improvement is observed, with a decrease in the proportion of areas affected by moderate drought and an increase in the proportion of drought-free areas. This suggests an overall improvement in vegetation health in the studied region over time. It is important to continue monitoring and implementing appropriate measures to maintain this positive trend and address drought variations in the region.

Prediction of drought indices for the Tigrigra watershed up to the year 2030 using machine learning models (xgboost model)

This step demonstrates a comprehensive process for reading, processing, predicting, and modifying pixel values in a series of TIFF images, utilizing various Python libraries including ‘rasterio’, ‘pandas’, ‘numpy’, and ‘xgboost’. Initially, the code installs the necessary ‘rasterio’ library and imports required libraries. It mounts Google Drive to access TIFF images stored therein. A function is defined to read pixel values from a TIFF image, specifically extracting the data of interest. This function is applied to several TIFF images from different years (2000, 2004, 2008, 2012, 2016, and 2020), filtering valid pixels (those within the range 0-255 and not equal to a specific invalid value) and storing them in individual DataFrames along with their row, column, and date information extracted from the file names.

These individual DataFrames are subsequently merged into a single DataFrame, grouping

pixel values by date to prepare training data for an XGBoost model. The training data consists of 'X_train' representing the years and 'y_train' representing the corresponding pixel values. An XGBoost model is then trained using these datasets with specific parameters like 'objective', 'eval_metric', 'max_depth', 'eta', 'subsample', 'colsample_bytree', and 'seed' set to fine-tune the model. The model undergoes a specified number of training rounds.

Once trained, the model predicts pixel values for future years, specifically 2024 in this example. The predictions are stored in a DataFrame, ensuring each pixel value is in a separate row. The process then shifts to modifying a base TIFF image (from 2012) by replacing its valid pixel values with zeros, verifying the absence of any invalid values, and finally updating these zeros with the predicted pixel values. The modified pixel values are reshaped to match the original image dimensions and written to a new output TIFF file, preserving the metadata from the original image. The modified image is then displayed using 'rasterio.plot.show', concluding the process. This workflow illustrates an integrated approach to temporal analysis and modification of geospatial raster data using machine learning.

	Hyperparameters	Best hyperparameter values
XGBOOST	Learning Rate	0.1
	Max Depth	6
	Gamma	0
	Reg Lambda	1

***Table 4**: Optimal Hyperparameters for XGBoost Model*

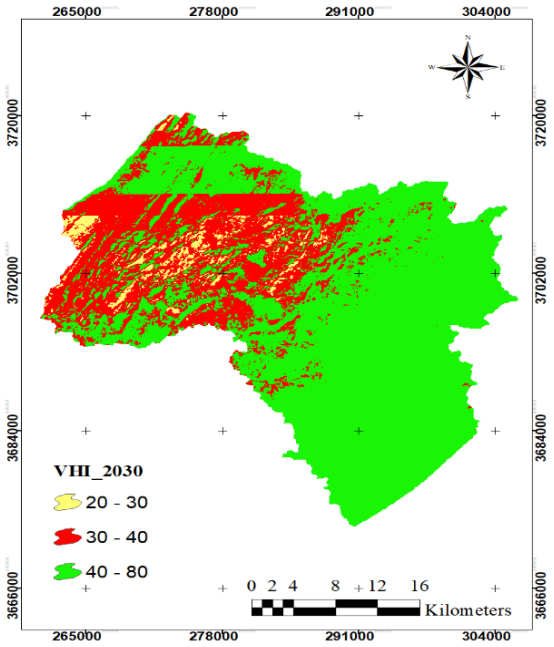

***Fig. 12**: VHI Prediction Map of the Year 2030*

Discussion and Interpretation

The spatial distribution of the Vegetation Health Index (VHI) for the year 2030 in the Tigrigra watershed reveals significant insights into the projected drought conditions of the region. The VHI values are categorized into three classes: 20-30 (moderate drought), 30-40 (mild drought), and 40-80 (no drought).

Spatial Analysis

The VHI map for 2030 (Figure X) indicates that the majority of the watershed is expected to experience conditions ranging from mild to no drought. Specifically, the areas classified as no drought (VHI 40-80) predominantly cover the southern and eastern parts of the watershed. These regions are characterized by relatively stable and healthy vegetation conditions, suggesting a lower impact of drought stress.

Conversely, the northwestern parts of the watershed exhibit moderate drought conditions (VHI 20-30), with a noticeable concentration of these areas depicted in yellow. This spatial pattern suggests that these regions are more vulnerable to drought stress,

possibly due to factors such as lower precipitation, higher temperatures, and variations in soil moisture retention capabilities.

Temporal Considerations

The temporal aspect of drought conditions, as analyzed through the VHI projections, underscores the dynamic nature of drought impacts on vegetation health. The moderate drought areas, although less extensive, highlight regions where vegetation may struggle, indicating the need for targeted drought mitigation strategies. The persistence of mild drought conditions across significant portions of the watershed further emphasizes the ongoing challenge of managing water resources effectively.

Implications for Drought Management

The findings from the VHI projections for 2030 have crucial implications for drought management in the Tigrigra watershed. The spatial heterogeneity of drought conditions necessitates a tailored approach to drought mitigation. Regions identified as vulnerable to moderate drought should be prioritized for interventions such as the implementation of efficient irrigation practices, drought-resistant crop varieties, and soil conservation techniques.

Moreover, the extensive areas classified as experiencing no drought provide an opportunity to leverage these regions for agricultural productivity, ensuring food security while managing water resources sustainably. Continuous monitoring using remote sensing technologies will be essential to update and refine drought management plans, adapting to changing climatic conditions and vegetation responses.

CONCLUSION

This study evaluated the temporal and spatial distribution of droughts, taking into account drought indices obtained from remote sensing, such as VCI, TCI, and VHI, as well as meteorological drought calculated by SPI (SPI-1, SPI-3, SPI-6, and SPI-12). Furthermore, from 2000 to 2022, assessments were carried out on the Tigrigra watershed using a restricted number of in situ meteorological stations. The key conclusions we came to are shown below.

(1) A considerable number of severe,

intense drought spells were recorded in 2000, 2003, 2007, 2009, 2014, 2019, and 2021, according to the SPI index statistics. When comparing SPI-1 and SPI-3 to long-term time scales (SPI-6 and SPI-12), significant variations in drought severity are seen. At the Ain Louh station, however, noteworthy findings are noted, indicating that the drought is more severe at smaller time scales (SPI-1) than it is at longer time scales. Overall, the findings demonstrated that regional differences in drought intensity caused by climate change were considerable.

(2) Based on the results of the VCI index, there were droughts in the Tigrigra watershed in 2004, 2008, 2012, and 2020. Droughts were more severe, with the northwest of the region typically seeing the lowest VCI values (between 0 and 30).

(3) According to the TCI index, drought became more severe from 2008 to 2016, especially in the northwest part. TCI values are more severe in the northwest part than in the south, except for a few years (2000, 2012, and 2016).

(4) The Vegetation Health Index (VHI) showed that the northwest part of the basin is in the moderate drought class by a percentage of 3%, while mild drought occupies 27% compared to the current 30%, whereas it is observed that 70% of the basin has no drought.

In conclusion, droughts have been tracked using both in-situ data and data obtained through remote sensing methods. Results for

VCI and TCI show contrasts, indicating that the southeast is experiencing more severe droughts than the northwest. Furthermore, areas with restricted access to meteorological stations and data have found great utility in remote sensing technology. As a result, knowing the characteristics of droughts in the study region requires a comprehension of the study's findings. The study
results provide useful information for addressing local and regional drought problems and designing drought mitigation plans.
Tigrigra watershed is prone to drought, especially in 2000, 2008, 2012, 2016, 2020, and 2022. The spatial distribution of the drought index highlighted episodes of moderate drought in 2000, 2008, 2012, 2016, and 2020. This index varies from 10 to 30, indicating moderate drought episodes.

(5) According to the analysis of the predicted drought degree map for the horizon of 2030, there is a slight increase.

References

[1]: Koem, C., Nusit, K., & Tantanee, S. (2022). "Spatial Distribution of Drought Hazard Mapping Based on AHP and GIS in Kampong Speu Province,", 442-450.

Cao, L., Li, P., Zhang, L., & Chen, T. (2008). Remote sensing image-based analysis of the relationship between urban heat island and vegetation fraction. The International Archives of the Photogrammetry, Remote Sensing and Spatial Information Sciences, 37, 1379-1384.

Carlson, T. N., & Ripley, D. A. (1997). On the relation between NDVI, fractional vegetation cover, and leaf area index. Remote Sensing of Environment, 62(3), 241-252.

Hereher, M., & El Kenawy, A. M. (2020). Exploring the potential of solar, tidal, and wind energy resources in Oman using an integrated climatic-socioeconomic approach. Renewable Energy, 161, 662-67.

Kogan, F. N. (1995). Application of vegetation index and brightness temperature for drought detection. Advances in space research, 15(11), 91-100.

Kogan, F. N. (1997). Global drought watch from space. Bulletin of the American Meteorological Society, 78(4), 621-636.

Kogan, F. N. (2001). Operational space technology for global vegetation assessment. Bulletin of the American Meteorological Society, 82(9), 1949-1964.

Kogan, F. N. (2001). Operational space technology for global vegetation assessment. Bulletin of the American Meteorological Society, 82(9), 1949-1964.

McKee, T. B., Doesken, N. J., & Kleist, J. (1993, January). The relationship of drought frequency and duration to time scales. In Proceedings of the 8th Conference on Applied Climatology (Vol. 17, No. 22, pp. 179-183).

Nalbantis, I., & Tsakiris, G. (2009). Assessment of hydrological drought revisited. Water resources management, 23, 881-897.

Palmer, W. C. (1965). Meteorological drought (Vol. 30). US Department of Commerce, Weather Bureau.

Sarkar, A., Kumar, V., Jasrotia, A. S., Taloor, A. K., Kumar, R., Sharma, R., ... & Roy, S. (2020). Spatial analysis and mapping of malaria risk in dehradun city India: A geospatial technology-based decision-making tool for planning and management. Geoecology of Landscape Dynamics, 207-221.

Shafer, B. A. (1982). Developemnet of a surface water supply index (SWSI) to assess the severity of drought conditions in snowpack runoff areas. In Proceedings of the 50th Annual Western Snow Conference, Colorado State University, Fort Collins, 1982.

Sharma, T. C., & Panu, U. S. (2010). Analytical procedures for weekly hydrological droughts: a case of Canadian rivers. Hydrological Sciences

Journal–Journal des Sciences Hydrologiques, 55(1), 79-92.

Singh, R. P., Roy, S., & Kogan, F. (2003). Vegetation and temperature condition indices from NOAA AVHRR data for drought monitoring over India. International journal of remote sensing, 24(22), 4393-4402.

Sobrino, J. A., Jiménez-Muñoz, J. C., & Paolini, L. (2004). Land surface temperature retrieval from LANDSAT TM 5. Remote Sensing of Environment, 90(4), 434-440.

Tucker, C. J. (1979). Red and photographic infrared linear combinations for monitoring vegetation. Remote Sensing of Environment, 8(2), 127-150.

Vicente-Serrano, S. M., Beguería, S., & López-Moreno, J. I. (2010). A multiscalar drought index sensitive to global warming: the standardized precipitation evapotranspiration index. Journal of climate, 23(7), 1696-1718.

Weng, Q., Lu, D., & Schubring, J. (2004). Estimation of land surface temperature–vegetation abundance relationship for urban heat island studies. Remote sensing of Environment, 89(4), 467-483.

West, H., Quinn, N., & Horswell, M. (2019). Remote sensing for drought monitoring & impact assessment: Progress, past challenges and future opportunities. Remote Sensing of Environment, 232, 111291.

Woli, P., Jones, J. W., Ingram, K. T., & Fraisse, C. W. (2012). Agricultural reference index for drought (ARID). Agronomy Journal, 104(2), 287-300.

Wukelic, G. E., Gibbons, D. E., Martucci, L. M., & Foote, H. P. (1989). Radiometric calibration of The Landsat Thematic Mapper thermal band. Remote sensing of environment, 28, 339-347.

USGS: https://earthexplorer.usgs.gov/

USGS, 2016. Landsat 4-5 TM and Landsat 7 ETM+ bands and their uses: https://www.usgs.gov/media/images/landsat-4-5-tm-and-landsat-7-etm-bands-and-their-uses

[2]: www.globalweather.tamu.edu